Journal of Power Sources 196 (2011) 4564–4572

Contents lists available at ScienceDirect

Journal of Power Sources

journal homepage: www.elsevier.com/locate/jpowsour

Basic properties of a liquid tin anode solid oxide fuel cell

Harry Abernathy[a,*], Randall Gemmen[a], Kirk Gerdes[a], Mark Koslowske[b], Thomas Tao[b]

[a] National Energy Technology Laboratory, 3610 Collins Ferry Rd., PO Box 880, Morgantown, WV 26507-0880, USA
[b] CellTech Power, LLC, 131 Flanders Rd., Westborough, MA 01581, USA

ARTICLE INFO

Article history:
Received 5 November 2010
Received in revised form
16 December 2010
Accepted 17 December 2010
Available online 7 January 2011

Keywords:
Solid oxide fuel cell
Oxygen diffusion
Tin
Liquid metal anode
Direct coal fuel cell

ABSTRACT

An unconventional high temperature fuel cell system, the liquid tin anode solid oxide fuel cell (LTA-SOFC), is discussed. A thermodynamic analysis of a solid oxide fuel cell with a liquid metal anode is developed. Pertinent thermochemical and thermophysical properties of liquid tin in particular are detailed. An experimental setup for analysis of LTA-SOFC anode kinetics is described, and data for a planar cell under hydrogen indicated an *effective* oxygen diffusion coefficient of 5.3×10^{-5} cm^2 s^{-1} at 800 °C and 8.9×10^{-5} cm^2 s^{-1} at 900 °C. This value is similar to previously reported literature values for liquid tin. The oxygen conductivity through the tin, calculated from measured diffusion coefficients and theoretical oxygen solubility limits, is found to be on the same order of that of yttria-stabilized zirconia (YSZ), a traditional SOFC electrolyte material. As such, the ohmic loss due to oxygen transport through the tin layer must be considered in practical system cell design since the tin layer will usually be at least as thick as the electrolyte.

1. Introduction

According to the International Energy Agency, world-wide demand for energy will continue to expand at rates of about 1.6% per year, which by 2030 will accrue to an overall 45% increase from 2006 [1]. Much of this energy will be electric-based, especially if plug-in hybrid vehicles significantly impact the transportation market. Even with the expected high growth of renewable energy technology, less than 5% of total power generation is expected to come from non-hydro renewables by 2030. The United States of America currently generates 68% of electricity from fossil fuels, with 44% of the total power coming from coal [2]. Hence, to achieve long term energy security, electric power production from coal can be expected to continue. To minimize the impact to the environment, CO_2 capture and sequestration technology has received significant global attention, and much work is being done to develop such capability [3,4].

To further minimize the cost and environmental impact of electric energy production from coal, higher efficiency systems are required. High temperature fuel cells, such as solid oxide fuel cells (SOFC), directly and efficiently convert fuel energy into electricity through electrochemical reactions (vs. combustion reactions that produce only heat). This technology can convert the chemical energy into electricity with a wide variety of fuel sources such as coal, biomass, and various hydrocarbon waste streams such as wood, paper, and plastics, into electricity [5]. An important consideration for any of these fuels is managing the impact of trace elements contained in these fuels on cell component degradation. At the high operating temperatures of conventional SOFCs (ca. 750–1000 °C), fuel contaminants such as sulfur and trace fuel constituents such as arsenic, phosphorus, and chlorine react with the anode materials thereby reducing the electrochemical reaction rates, increasing the electric ohmic resistances of their materials, and causing material phase changes that can weaken materials and result in mechanical failure [6–8].

Mitigating the impact of such reactions requires reduction of the trace element loading via filters and sorbent catalysts, or increasing the robustness of the anode materials to improve tolerance for exposure to contaminant materials. In this paper we consider a metal anode material that resides as a liquid layer between the fuel gas and the cell electrolyte, as shown in Fig. 1. An example of such technology is CellTech Power's direct conversion fuel cell technology based on the liquid tin anode solid oxide fuel cell (LTA-SOFC) [5,9–13]. This technology has been demonstrated to operate on gaseous, liquid, and solid carbonaceous fuels without fuel processing, reforming or sulfur removal. System efficiency is expected to be 61% for coal-based systems [10]. Current state of the art single cell performance shows a power density of 170 mW cm^{-2} on hydrogen and JP-8 fuel [13].

The anode in Fig. 1 is a liquid layer that fully covers the active oxygen exchange area between the electrolyte and the anode. The anode serves as a buffer against fuel contaminants, as it blocks

* Corresponding author at: National Energy Technology Laboratory, 3610 Collins Ferry Rd., PO Box 880, Morgantown, WV 26507-0880, USA.
Tel.: +1 304 285 4632; fax: +1 304 285 0903.
E-mail address: Harry.Abernathy@netl.doe.gov (H. Abernathy).

0378-7753/$ – see front matter © 2011 Elsevier B.V. All rights reserved.
doi:10.1016/j.jpowsour.2010.12.089

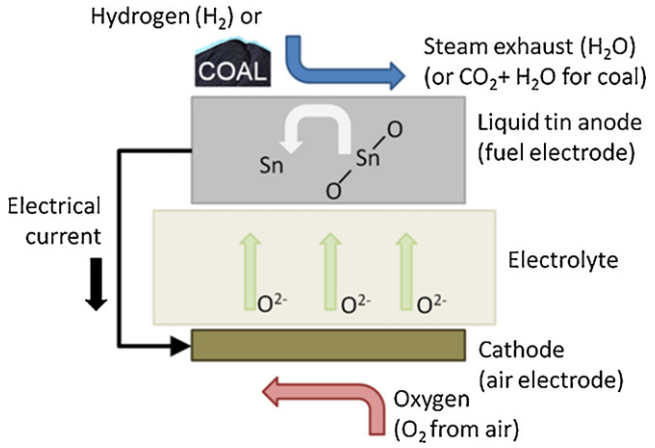

Fig. 1. Liquid metal anode SOFC, with tin as the metal.

the transport of insoluble or slag-forming constituents to the electrolyte and impedes the transport of soluble fuel contaminants, thereby reducing the rate of contaminant reactions with the electrolyte. Fuel contaminants that can be electrochemically oxidized could also provide a fuel source [10]. It is also postulated that the electrolyte surface usage efficiency, η_{es}, is improved over existing porous solid anode technology because the liquid layer fully covers the electrolyte. Hence, oxygen reactions can be expected to occur over the full surface of the electrolyte when using a liquid anode, instead of only around triple phase boundaries between the fuel, anode, and electrolyte.

Some technical issues require attention before commercial deployment of the liquid anode SOFC. Foremost is developing an understanding of how oxygen and fuel react within the liquid metal electrochemical system. In particular, electrochemical oxidation kinetics, compared to conventional SOFCs, can be relatively slow for liquid metal anodes, which diminishes the benefit of high interfacial contact [12]. Details of the kinetics of the oxygen transfer at the liquid metal–electrolyte and the liquid metal–fuel interface need to be studied. Also, oxygen transport within the liquid anode is not fully understood. Quantitative evaluation of oxygen transport through the metal anode as well as across the two interfaces will identify the rate-limiting transport step for given cell geometries as well as indicate probable methods of cell improvement. This paper reviews relevant data for liquid tin-based SOFCs and describes our measurements of oxygen transport kinetics.

Section 2 of this paper presents thermodynamic considerations for the operation of a liquid metal anode SOFC. Because the metal anode acts only as an intermediary in the overall thermodynamic state change for fuel oxidation, the results are general to any liquid metal anode SOFC. Special consideration is given to operation in battery mode, i.e., when the metal is oxidized in the absence of another fuel source. Section 3 compiles relevant physical and chemical properties of tin. Section 4 describes the experimental approach being used to study diffusion transport and reaction kinetics, and presents available experimental data. Section 5 provides a summary of the work and provides concluding remarks.

2. Fundamentals of liquid anode SOFC operation

In the operation of a liquid metal–SOFC system, the liquid anode will participate as an 'intermediary' for the oxidation of fuel delivered to the fuel cell. As an example, consider a tin-based SOFC fueled by hydrogen. This case can be written concisely using the following reaction steps on the anode side:

$$Sn + xO^{2-} \rightarrow Sn[O_x]_{Sn} + 2xe^- \quad (2.1)$$

$$xH_2 + Sn[O_x]_{Sn} \rightarrow Sn + xH_2O \quad (2.2)$$

Reaction (2.1) occurs at the anode–electrolyte interface. Reaction (2.2) occurs at the fuel–anode interface. In the above equations, O^{2-} is an oxygen ion supplied to the anode through the electrolyte. $[O_x]_{Sn}$ is a state of oxygen within the metal anode (tin for the reactions shown in these equations). The use of the parameter 'x' is used because the state of oxygen in the tin is not definitely known and may vary with operating conditions (e.g., the atmosphere, the exact tin alloy composition). Oxygen may associate tightly with Sn to form an oxide or suboxide, or loosely in a dissolved oxygen state within the liquid metal. Although several $[O_x]_{Sn}$ states can be considered, for operation as a fuel cell, the major requirement is that the oxygen is part of a soluble (i.e., not solid) species that can migrate through the liquid tin to the anode–fuel interface to undergo Reaction (2.2).

Adding Eqs. (2.1) and (2.2) generates the global anode reaction between hydrogen and the oxygen anion ($H_2 + O^{2-} \rightarrow H_2O + 2e^-$). Such an overall change is the same for any liquid metal-based SOFC anode system, although the value of 'x' in the detailed Reactions (2.1) and (2.2) will be particular to a given metal-oxide complex. For example, a liquid Ni anode with similar functionality for which 'x' is close to 1 is conceivable. Further, the overall reaction is identical to other SOFC technology (e.g., porous Ni–YSZ based anode technology), and in fact is generally applicable to any operating oxygen-ion-conducting fuel cell.

2.1. Ideal potential

Given the above analysis, we can directly conclude that the ideal potential for a liquid metal anode SOFC will be the same as any other fuel cell, and when operating on hydrogen fuel the ideal potential can be written as:

$$E_N = \frac{-\Delta G^o}{2F} + \frac{RT}{2F} \ln\left(\frac{a_{H_2-A} a_{O_2-C}{}^{1/2}}{a_{H_2O-A}}\right) \quad (2.3a)$$

or more generally as,

$$E_N = \frac{RT}{4F} \ln\left(\frac{a_{O_2-C}}{a_{O_2-A}}\right) \quad (2.3b)$$

In Eq. (2.3), E_N is the ideal Nernst voltage, ΔG^o is the change in the standard state Gibbs free energy for the overall reaction $H_2 + (1/2)O_2 \rightarrow H_2O$, which is only a function of temperature, a_{z-y} is the gas phase activity (partial pressures when assuming ideal gas behavior) of a supplied reactant ('z') present in either the cathode or anode ('y') gas, R is the universal gas constant, T is absolute temperature, and F is the Faraday constant.

2.2. Anode gas–liquid metal equilibrium

Anode gas-phase species are assumed to be in equilibrium with their counterparts in the liquid anode. Such equilibrium occurs when the chemical potential of a species in the gas phase is equal to the chemical potential of that species in the liquid metal. For oxygen within the anode, we can write at equilibrium:

$$\mu_{O_2-A} = \mu_{O_2-M}$$
$$\mu^o_{O_2} + RT \ln(a_{O_2-A}) = \mu^o_{O_2} + RT \ln(a_{O_2-M}) \quad (2.4)$$
$$a_{O_2-A} = a_{O_2-M}$$

where μ_{O_2-M} stands for the chemical potential of O_2 in the liquid metal anode and a_{O_2-M} is the activity of O_2 within the liquid metal.

The concentration of H_2 and H_2O present in the anode gas corresponds to gas phase oxygen activity. The gas phase oxygen activity will control the activity of oxygen within the liquid metal, regardless of the dominant form of oxygen existing within the liquid metal

anode (e.g., oxide, suboxide, or dissolved oxygen). As a result, we can write equivalently for Eq. (2.3b):

$$E_N = \frac{RT}{4F} \ln\left(\frac{a_{O_2-C}}{a_{O_2-M}}\right) \quad (2.5)$$

In summary, under equilibrium conditions at open circuit, the activity of oxygen within the tin is uniform everywhere, and equal to the activity of oxygen in the anode gas chamber, and provides an equivalent value for E_N as that given by Eq. (2.3b).

2.3. Liquid metal–metal oxide equilibrium

The above equations are general and are applicable for any concentration of oxygen within the anode. At sufficiently large concentration of oxygen in the anode, a solid metal-oxide secondary phase can form and equilibrate with the liquid metal and oxygen present in the anode. As shown above, when oxygen in the gas is in equilibrium with oxygen in the liquid metal, the source of oxygen in the reaction can be considered as from either the gas or the metal:

$$M + (x/2)O_2 \rightarrow MO_x \quad (2.6)$$

At equilibrium, the change in Gibbs free energy is zero:

$$\Delta G = 0 = \Delta G^o_{M-MO_x} - RT \ln\left(a_{O_2-A}{}^{x/2}\right) \quad (2.7)$$

Solving for the activity of molecular oxygen in the anode, we have:

$$a^{x/2}_{O_2-A} = \exp\left(\frac{\Delta G^o_{M-MO_x}}{RT}\right) \quad (2.8)$$

Hence, at a point where both metal and metal-oxide phases are present within the liquid metal, a specific activity of oxygen within the anode gas is expected (for a specific operating temperature) as shown in Eq. (2.8). Eq. (2.3b) indicates that the ideal potential will only be a function of the cathode oxygen activity and operating temperature as long as the some of the anode remains reduced. It is then possible to write:

$$E_N = \frac{-\Delta G^o_{M-MO_x}}{2F} + \frac{RT}{4F} \ln\left(a_{O_2-C}\right) \quad (2.9)$$

2.4. Estimates for non-equilibrium operation

In summary, the general equation for determining the ideal potential is given by Eq. (2.3b). If it is known that both metal and metal-oxide phases are present (oxygen activity at or above the solubility limit), then the Nernst equation, (2.9), can be used (e.g., in "battery mode" where only M to MO_x conversion is possible). Alternatively, if H_2 (or some carbon-based fuel) is available for reaction, then the Nernst equation, (2.3), for H_2 to H_2O (or C to CO_2) conversion can be used. As an example, Fig. 2 shows both equations plotted over a range of temperatures for a tin-based SOFC system, where a specific hydrogen content of 97% is assumed. For such high hydrogen concentrations, the gas phase anode oxygen mole fraction is very low (2.7×10^{-18} at 1000 °C) and the tin is effectively reduced.

Fig. 3 shows for fixed temperature, how oxygen content (O_2/Sn ratio) in the anode controls the ideal potential. For the 1000 °C case, below about 0.25% O_2:Sn the oxygen activity increases with increasing oxygen content until the gas phase oxygen mole fraction is $\sim 8.8 \times 10^{-14}$. As oxygen is added to this system, the oxygen activity within the metal anode becomes fixed until all Sn is converted to SnO_2 (ca. O_2:Sn = 1.0). During this process, the Nernst potential remains fixed at 0.8 V. For oxygen content of O_2:Sn > 1, the anode oxygen activity will rapidly increase and the ideal potential will decrease.

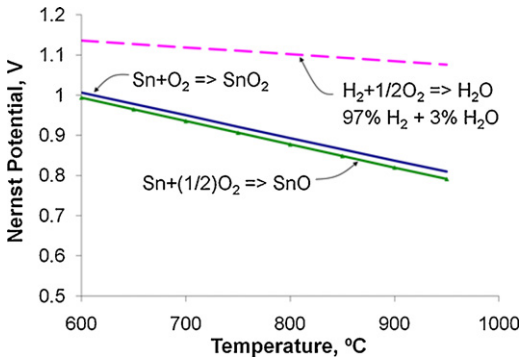

Fig. 2. Nernst potentials for $Sn + O_2 \rightarrow SnO_2$, $Sn + (1/2)O_2 \rightarrow SnO$, and $H_2 + (1/2)O_2 \rightarrow H_2O$. Pressure = 1 atm. Cathode air O_2 partial pressure = 0.21 atm.

While the above theoretical equilibrium analysis is helpful for estimating fuel cell performance, in a real operating fuel cell ($i > 0.0\,A\,cm^{-2}$), the system is not in a static equilibrium, and a higher activity of oxygen will exist within the liquid metal anode than that within the anode gas stream. Specifically, the activity of oxygen near the liquid–electrolyte interface will be greater than that near the gas–liquid interface due to diffusion resistance through the liquid metal. At some level of current density, interfacial oxygen activity can increase sufficiently above that in the anode gas (which can be maintained low in the presence of fuel), and a metal oxide phase will form. As most metal oxides have high melting temperatures and may or may not be good ionic or electronic conductors, their formation at the electrolyte interface will reduce the operating potential.

2.5. Operational losses

In the analysis of common SOFC performance where the anode is supplied gaseous fuel and the cathode is supplied air, the cell voltage at a given current load is often represented as:

$$V_{cell} = E_N - \eta_{aa} - \eta_{ca} - \eta_{ac} - \eta_{cc} - \eta_R \quad (2.10)$$

in which η_i is the loss in voltage due to particular mechanism 'i': a_a = anode activation loss; c_a = cathode activation loss; a_c = anode concentration loss; c_c = cathode concentration loss; and R = ohmic loss. These losses also exist for the liquid anode SOFC fuel cell; however the exact physical contributions to each of these components for a liquid anode SOFC are unique.

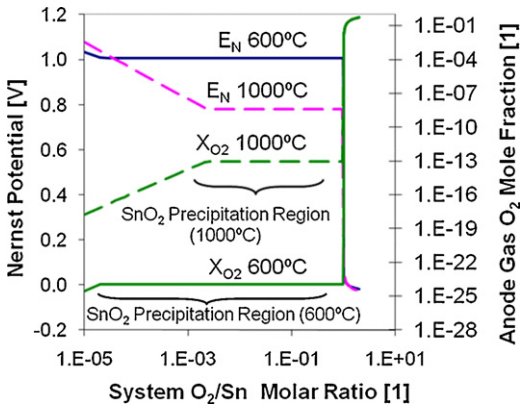

Fig. 3. Nernst potentials and anode oxygen mole fractions for a tin + oxygen system with varying anode oxygen:tin molar content, cathode oxygen mole fraction = 0.21, P = 1 atm., and two different temperatures. Concentration data for oxygen in tin calculated using FactSage™ software.

Table 1
Properties and abundances of common metals.

Metal	T_m, °C	T_b, °C	Abundance [14], ppm of crust	Annual production [15], tons	Price [15], $ kg^{-1}
Aluminum	660	2520	83,000 (8.2%)	36.9 million	1.72
Antimony	631	1587	0.20	187,000	5.06
Bismuth	271	1564	0.063	7300	16.28
Cadmium	321	767	0.10	18,800	2.68
Copper	1085	2563	79	15.8 million	5.21
Indium	157	2073	0.05	600	390.00
Lead	328	1750	7.9	3.9 million	1.74
Tin	232	2603	2.5	307,000	13.88
Silver	962	2163	0.079	21,400	470.63
Zinc	420	907	79	11.1 million	1.72

One additional loss mechanism unique to the liquid anode–SOFC system pertains to the kinetics of fuel oxidation at the anode–gas interface, written globally for tin in Eq. (2.2). Should the fuel oxidation reaction be sluggish relative to oxygen transport in the liquid metal, the oxygen in the bulk liquid metal will build up, with the cell voltage being determined by Eq. (2.5). For a finite change in the activity of a_{O_2-M} in the liquid anode (say above the equilibrium concentration), the change in cell voltage will be:

$$\Delta E_N = \eta_I = \frac{RT}{4F} \ln\left(\frac{a_{O_2-M}}{a^*_{O_2-M}}\right) \tag{2.11}$$

in which η_I is the interfacial loss, and $a^*_{O_2-M}$ is the activity of dissolved oxygen at equilibrium (zero current load). Hence, under current loading, the activity of dissolved oxygen at the interface will increase above equilibrium conditions thereby causing a reduction in cell voltage. If we assume a linear variation of dissolved oxygen activity with current load, e.g., $a_{O_2-M} = a^*_{O_2-M}(1 + i/i_{Ix})$, then Eq. (2.11) becomes:

$$\eta_I = \frac{RT}{4F} \ln\left(1 + \frac{i}{i_{Ix}}\right) \tag{2.12}$$

In Eq. (2.12), i_{Ix} can be interpreted to be the effective exchange current density for the interface kinetics. As long as the current load, i, is much lower than this interface exchange rate current, the loss due to this mechanism will be small. It remains to be seen whether a linear relation for the variation of activity of oxygen at the interface is valid, but given the first order relation shown in Eq. (2.12) for dissolved oxygen, it is considered a viable first-order approximation.

Finally, oxygen mass transport through the liquid metal layer is an additional loss. The speed of oxygen transport depends upon the diffusivity of oxygen through the liquid metal and the amount of dissolved oxygen species, the maximum of which is determined by the oxygen solubility limit for the given metal. When the current density exceeds the anode's ability to transport oxygen to the fuel–anode interface, metal oxide will begin to precipitate to meet the additional current demand, again reducing the operating voltage. The transport of a small amount of metal oxide phase through the liquid metal may be theoretically possible, depending on the size of the metal oxide particle, the relative densities of the liquid metal and metal oxide, the cell geometry, and the relative ease by which the metal oxide layer can be dislodged from the electrolyte surface. Assuming some solid metal oxide moves across the anode, some of it may redissolve into the liquid metal as the local oxygen activity drops below the oxygen solubility limit. This scenario seems unlikely, would require a more complex transport model, and should be avoided in an operating LTA-SOFC system to avoid unnecessary complications.

2.6. Battery mode

If the metal anode material is readily oxidizable, then it can also act as a source of fuel and can offer another reaction pathway with a unique Nernst potential. If no fuel is present for removing oxygen from the liquid metal (e.g., tin), then the metal–SOFC system becomes a battery whereby the finite quantity of metal present will be steadily oxidized until essentially all available metal becomes a metal oxide phase (e.g., SnO_2). Over the course of consumption of the metal, the amount of oxygen gradually increases until the metal is saturated with oxygen at an activity equal to that of the cathode. Based on Eq. (2.9), this must occur after essentially all metal is oxidized and any excess oxygen exists within the anode gas at an activity equal to the cathode activity. This inherent battery capability provides an extra source of capacity to the system that can buffer fluctuations in fuel gas supply, thereby providing a more stable power output. The limit to which the cell can act as a battery is determined by the oxygen solubility limit of the metal and the reversibility of the formation of the metal oxide phase. Operating below the solubility limit of oxygen in the liquid metal is safe, but if the formation of a secondary metal oxide phase is irreversible, it should be avoided, as it would permanently depress the operating voltage of the SOFC.

3. Tin thermophysical and thermochemical properties

The foregoing discussion has been generalized for any liquid metal anode system, with some specific cases given for tin. Since the authors' work is focusing on the use of tin for the anode, available property data for tin are given here. Although tin has been extensively studied regarding its solid phase properties, and has been used in many applications such as containers, solders, and coatings, the specific liquid phase material properties pertinent to this electrochemical application have not been well reported in literature. For example, a wide range in reported oxygen solubility values exists for liquid tin.

3.1. Basic property data

Table 1 compares the melting and boiling point of tin with those of various common metals with melting points below 1100 °C [14,15]. Tin is a good candidate liquid anode material for SOFCs because of its combination of low melting temperature (~231.88 °C) and high boiling temperature (2603 °C) [16]. The melting point of 232 °C is low relative to a typical SOFC operating temperature of 1000 °C and facilitates higher oxygen solubility. The high boiling point provides low vapor pressures (ca. 0.7 Pa at 1000 °C) and therefore low vapor loss when operating at SOFC temperatures. Although tin is not the most abundant commodity metal, the tin industry is very well-established, producing over one quarter of a million tons of tin annually [15].

Table 2 is a compilation of thermophysical property data for tin, including available values for oxygen, sulfur, and hydrogen solubility [16–19]. As will be shown in Section 4, the existence of hydrogen in the tin may explain the faster transient behavior identified in the present tests. The solubility of sulfur is attractive since the tin bath can tolerate a higher sulfur content in the fuel stream than

Table 2
Thermophysical property data for liquid tin.

Property	Temperature, °C	Value
Surface tension [16]	231.88	544 dynes cm^{-1}
Viscosity [16]	231.88	1.85 mN s m^{-2}
Expansion on melting [16]	231.88	2.3%
Density [17]	800	6.58 g cm^{-3}
	1000	6.48 g cm^{-3}
Resistivity [18]	800	62.1 μΩ cm
	1000	67.1 μΩ cm
Gas solubility—oxygen [16]	536	0.00018 wt%
	750	0.0049 wt%
Gas solubility—hydrogen [19]	1000	0.04 cm^3 H_2/100 g Sn
	1300	0.36 cm^3 H_2/100 g Sn
Gas solubility—sulfur [45]	800	4.5 at%
	1000	8.0 at%

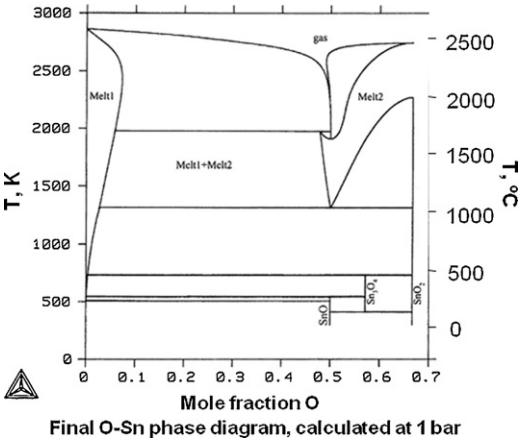

Fig. 4. Phase diagram for Sn–O (Celcius scale added) [22].

can nickel. The sulfur will dissolve and disperse into the liquid tin instead of staying adsorbed on the tin surface or forming a tin sulfide (at least until it is oxidized or the solubility limit is exceeded). The sulfur can then be oxidized as an additional fuel since it does not immediately hinder the catalytic properties of the liquid tin, in contrast with nickel.

The electronic resistance of liquid tin is very small at SOFC operating temperatures, especially considering the larger anode–electrolyte contact area used for liquid anode SOFCs. Electron flow through the tin to the current collector should thus be sufficient. Surface tension measurements of drops of liquid tin were also reported by Ricci et al. as a function of temperature and oxygen partial pressure [20]. Surface tensions between 520 and 550 dynes cm^{-1} are reported between temperatures of 352 and 827 °C at low oxygen partial pressure for several heating/cooling rates. In the design of LTA-SOFC systems, surface tension affects the tin/electrolyte contact angle for a given geometry. For thin layers of tin, extra pressure may be required to improve contact between the tin and the electrolyte. Viscosity numbers are pertinent if circulation of the liquid tin is required for processing (e.g., removal of slag, further reaction with fuel).

3.2. Sn–O phase diagram

The phase diagram for oxygen and tin provides fundamental information on the possible states for oxygen in tin. However, a review of available data shows variability in oxygen solubility in tin. An early version of the Sn–O phase diagram presented by Hansen [21] did not define the oxygen solubility at low concentrations, which was indicated by dashed boundary lines. A more recent version of the phase diagram for the Sn–O system determined by Cahen et al. [22] is given in Fig. 4. The thermodynamic model used for the liquid phase of this diagram is Hillert's partially ionic liquid model. The electronic structure of the liquid tin via such a model allows for the solubility of oxygen [O] in the liquid (Melt1) at low concentrations of oxygen. The solubility limit of oxygen is ~2% at 1000 °C. Above this concentration of oxygen, SnO_2 begins to precipitate (SnO_2 m.p. = 2000 °C).

The solubility of oxygen in tin was also investigated by Belford and Alcock [23] and is presented in Table 3. The solubility values from EMF measurements were only obtained between 500 °C and 751 °C. Eq. (3.1) is derived from the experimental data where N[Sn] is the mole fraction of tin and the term $N^{1/2}$[Sn]c_s corresponds to the equilibrium constant for the reaction $(1/2)SnO_2(s) = (1/2)Sn(l) + [O]$. By fitting Eq. (3.1) into the form of the error equation (3.2), the two can be used to predict the solubility in the temperature range of 232–1100 °C. This is possible provided the conditions of oxygen in tin follow Henry's law and the activity of tin obeys Raoult's law for values up to 1.0 at% [O].

$$\log_{10}(N^{1/2}[\mathrm{Sn}]c_s) = -5670/T + 4.12 \quad (3.1)$$

$$\log_{10}(N^{1/2}[\mathrm{Sn}]c_s) = -(5730 \pm 210)/T + (4.19 \pm 0.23) \quad (3.2)$$

Experimental work was performed at CellTech Power in an attempt to validate the oxygen solubility in the tin anode fuel cell and to potentially narrow down the range of values found in the literature. CellTech Power Gen 2.0 cells were tested electrochemically to determine the voltage decay at various load values in an inert anode environment. Since the conversion of Sn to SnO_2 is calculated to occur below 0.78 V, the [O] can be calculated by the $[O^{2-}]$ flux through the electrolyte at each current value. Based on this experimental method, the oxygen solubility was shown to be closer to 0.8 at% at the 1000 °C operating temperature.

Finally, the present authors determined the oxygen solubility of the Sn–O system using the thermodynamic modeling software, FactSage™ version 5.6 [24,25], based on the available thermodynamic data for the Gibbs free energy of formation for tin oxides [26–31]. Fig. 5 shows oxygen solubility through a temperature range of $-173 < T < 2727$ °C, with a maximum of ~10% occurring at 1600 °C. At the fuel cell operating temperature of 1000 °C, the oxygen atom solubility is predicted to be about 0.5%, which is similar to that provided by Belford and Alcock [23], but much different than that shown by Cahen et al. [22]. Differences in the phase diagrams demonstrate the variability in the understanding of the solubility limit of oxygen and other species in tin. The FactSage™ analysis does not account for a second liquid phase or intermediate compounds that create a miscibility gap at 1040 °C (as evident in Fig. 4). The gas phase regions also show some differences in the maximum oxygen solubility. The shape inconsistency of the (Sn-liq + gas) boundary can likely be attributed to the assumptions used for the gas phase mixture and the thermodynamic data available in FactSage™.

Table 3
Oxygen solubility in tin [23].

Temperature, °C	at% [O]	wt% [O]	Method
536	0.0012	0.0002	Measured
600	0.0042	0.0006	Measured
700	0.0190	0.0026	Measured
751	0.0360	0.0048	Measured
800	0.0708	0.0096	Calculated
850	0.1220	0.0165	Calculated
900	0.2020	0.0273	Calculated
950	0.3200	0.0432	Calculated
1000	0.4880	0.0660	Calculated
1050	0.7230	0.0976	Calculated
1100	1.0390	0.1403	Calculated

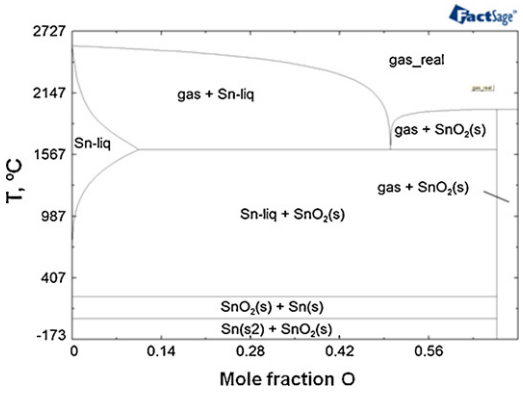

Fig. 5. Solubility of oxygen in Sn–O system as a function of temperature. Total pressure = 1 bar.

The molten tin anode layer in an SOFC acts as a conduit for oxygen between the electrolyte and the fuel. The oxygen solubility limit in tin is thus a significant operating parameter since the effective oxygen conductivity of the tin layer is directly proportional to the amount of oxygen that can be pumped into the tin without causing the formation of a solid tin oxide species. Differences in solubility from 0.5 to 2.0 at% represent a fourfold increase in the oxygen-carrying capability, which could limit the minimum area or maximum thickness of the tin layer depending on the cell geometry.

Although the oxygen solubility limit cannot be absolutely resolved as yet, several regions within the phase diagrams are pertinent to understanding oxygen transport within the tin-anode SOFC. All data show a lower solubility limit of oxygen in liquid tin for temperatures $477 < T < 1600\,^{\circ}C$ and oxygen atom concentrations are less than ca. 2% at 1000 °C. Addition of oxygen beyond the solubility limit will precipitate a phase of SnO_2, Sn_xO_{1+x}, or SnO depending on the operating temperature. Differential scanning calorimetry measurements were made by Bonicelli et al., confirming that only SnO_2 is found at temperatures >525 °C when disproportioning SnO [32].

As a result of the work of Bonicelli et al. showing SnO_2 present above 525 °C, it is prudent to examine some of the thermochemical properties for SnO_2 systems. Tin dioxide is an n-type wide gap semiconductor with a bulk conductivity on the order of 0.3 S cm^{-1} at 1000 °C [33]; however, this number reflects dense SnO_2. A less dense layer of SnO_2 can exhibit a conductivity that is multiple orders of magnitude lower, especially at higher temperatures [34]. This decline in conductivity explains why the power output of a tin-based SOFC would significantly decline even with the formation of thin layers of SnO_2. A chemical diffusion coefficient for oxygen in SnO_2 was reported by Kamp et al. [35]. Through a temperature range of 700–1000 °C, the chemical diffusion coefficient is expressed as $D_o = 0.02\ cm^2\ s^{-1} \exp(-0.9\ eV/kT)$. The density of SnO_2 at room temperature is 7.0 g cm^{-3} (compared to 7.3 g cm^{-3} for metallic tin at 25 °C). However, in the higher temperature operating range for SOFCs, SnO_2 is denser than molten tin: ρ for SnO_2 is calculated to be approximately 6.98 g cm^{-3} while that for molten tin is 6.6 and 6.5 g cm^{-3} at 800 °C and 1000 °C, respectively [17,36]. Since SnO_2 is denser, the operating voltage of the cell must be closely monitored to avoid the formation of the oxide at the electrolyte–anode interface (especially in planar designs with the tin bath resting on top of the electrolyte), as the oxide layer will not float to the top to allow for its possible removal.

There are still differences in the literature values, both experimental and predicted, especially for the oxygen solubility in liquid tin. There is a need for a complete scientific understanding of this interaction as applied to fuel cell applications. Information on physical properties including contact angle and surface tension for high temperatures and various environments (oxidizing to reducing) have also not been well-defined, but are critical to design of systems with long term stability.

4. Experimental data

4.1. Experimental setup

One of the objectives of the LTA-SOFC research performed at NETL is to clarify the oxygen transport mechanism through the liquid tin. Since the goal is to accurately measure anode kinetics and not to maximize performance, the sample cell was designed with a convenient planar geometry. A planar configuration simplifies calculations and accommodates quick changes in electrode dimensions, fuel flow, etc. to isolate different components of anode operation. The initial experimental setup shown in Fig. 6(a) utilized a ~30 mm diameter electrolyte-supported button cell with a screen-printed LSM cathode and a 6–20 mm thick layer of molten tin (99.999%, Alfa Aesar). Both yttria-stabilized zirconia (YSZ) and Hionic™ (purchased from Fuel Cell Materials, Ltd.) electrolyte supports of ~120 μm thickness were tested. The cell was mounted to

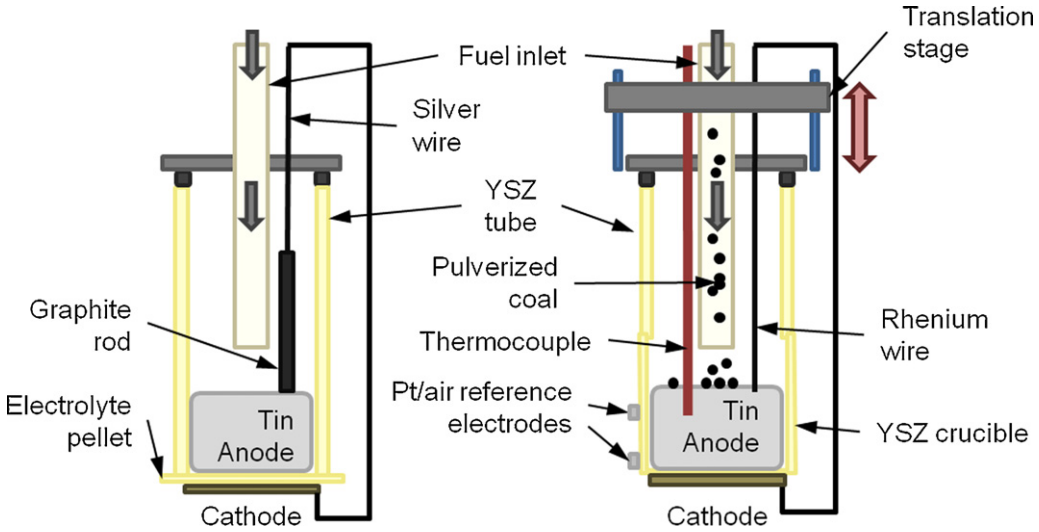

Fig. 6. Liquid tin anode experimental setup. (a) Initial setup using an electrolyte-supported cell attached to a YSZ tube. (b) Final setup with YSZ crucible attached to the YSZ tube. The thermocouple and anode current collector rod are mounted to separate, independent translation stages.

the bottom of a YSZ tube (6 mol% Y_2O_3, McDanel Advanced Ceramic Technologies) using two coats of Aremco 885 ceramic sealant, each cured at 265 °C for 2 h. Current collection on the screen-printed cathode was performed using a platinum mesh attached with a platinum ink. The voltage and current leads were silver wire welded to the platinum mesh.

For current collection on the anode side, a graphite rod was brought into contact with the 25 mm diameter molten tin bath. Material selection for electrical contact with the liquid tin is significant, in that the material must be relatively insoluble in liquid tin (to prevent alloying) and it must survive, chemically and mechanically, in a reducing environment up to 1000 °C. Common SOFC contact materials such as platinum, gold, and silver are all soluble in liquid tin. And while carbon is certainly a candidate fuel for a liquid anode SOFC, the authors found that as long as a more reactive fuel is present (e.g., H_2, pulverized coal) and as long as the current density is extremely low, the graphite is kinetically stable. The free end of the graphite rod was wrapped in two silver lead wires—one for delivering current and the other for measuring cell potential. An alumina tube inside the larger zirconia tube acted as the anode fuel inlet line, delivering fuel within 8 mm of the top of the liquid metal–gas interface. The fuel feed can either be hydrogen gas or a solid fuel (activated carbon, pulverized coal). The solid fuel can be delivered through a lock hopper attached to the top of the tube. For the diffusion measurements reported here, humidified UHP hydrogen (3% H_2O) was used as a fuel instead of solid fuel particulates. Hydrogen fuel was selected because it is easy to deliver to the sample and because it lowers the risk of contaminating the tin with possible impurities in solid fuel sources. Contamination was not desired for these measurements since baseline oxygen diffusion coefficients were desired for pure tin.

The cell potential was continuously monitored using a National Instruments Compact FieldPoint module. Electrochemical performance data were collected with a Solartron 1260/1287 Frequency Response Analyzer/Electrochemical Interface or a Solartron Modulab system. To measure the oxygen diffusion rate through the tin layer, the voltage across the cell was stepped 20 mV off of OCV while monitoring the current response. The response of the cell, when diffusion-limited, demonstrates an initial spike in current as the tin at the electrolyte–anode interface is oxidized, followed by a decay as the oxygen diffuses away from the interface until the oxygen activity in the tin reaches the steady-state value dictated by the 20 mV step in potential. The current response was also monitored as the potential was stepped back to OCV. To solve for the oxygen diffusion coefficient, the experiment was assumed to act as a layer of thickness $2l$ with an initial oxygen concentration of zero and with one surface (the anode/electrolyte interface) being held at concentration c_o (determined by the cell potential). The solution to this one dimensional diffusion problem can be found (for the thermal transport equivalent) in Carslaw and Jaeger [37]. The total charge passed through the sample was calculated up until the sample reached equilibrium at the new potential. For the time required for 92.88% of the total charge to pass into the tin layer, the parameter $D_o t/l^2$ is equal to one.

4.2. Results and discussion

Fig. 7(a) shows the average of 10 cycles of stepping 20 mV from an OCV of 0.907 V and holding for 15 min followed by stepping to 20 mV back to OCV and holding for 15 min. The sample was under hydrogen (with 3% H_2O) at 800 °C. When the voltage was stepped away from OCV, the system eventually reached a nonzero steady state current. This is the operating current for the fuel cell at that voltage, and its value was subtracted out when calculating the necessary amount of charge passing into the tin to reach the steady state oxygen concentration. In the absence of a fuel (i.e., when the sample is operating in battery mode), the current would decay to zero, as the oxygen concentration in the tin bath reaches the equilibrium value for the applied voltage. Regardless of fuel condition, the current will decay to zero when stepping back to OCV.

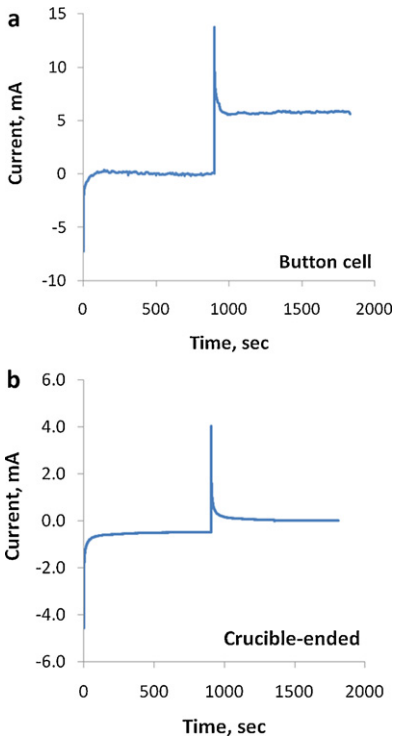

Fig. 7. Current response to a 20 mV potential step from and then back to OCV of liquid tin anode SOFC under H_2 flow at 800 °C for (a) the button cell sample and (b) the crucible-ended sample. The lower noise in (b) indicates a lack of air leaking into the tin layer.

As stated above, the OCV at 800 °C for the sample used in Fig. 7(a) was only 0.907 V, which is well below the ideal Nernst potential for hydrogen of 1.10 V (1.07 with 3% H_2O). The current response data, even after averaging 10 potential step cycles together, was very noisy. Further, the OCV had decreased to 0.900 V during the experiment, indicating deterioration of the cell. Upon removal of the sample from the furnace, the tin layer contained a white precipitate between the tin slug and electrolyte layer, as shown in Fig. 8.

Fig. 8. Photograph of the surface of tin slug in contact with the electrolyte for the button cell sample. The ring of wing around the circumference is SnO_2.

The precipitate was primarily located around the circumference of the tin and was progressing inward. X-ray diffraction of the powder indicated the SnO_2 phase. The ceramic sealant attaching the button cell to the YSZ tube had leaked during the test, forming an oxide layer, which shortens the diffusion path through the tin layer itself while adding a physical barrier to oxygen transport from the electrolyte into the liquid tin.

To eliminate the leaking issue, the sample cell design was changed to that shown in Fig. 6(b). Instead of a button cell, a YSZ crucible (6 mol% Y_2O_3, McDanel Advanced Ceramic Technologies) with a ~1.5 mm wall thickness was attached to the YSZ tube again using Aremco 885 ceramic paste. A small 4 mm lip was machined around the end of the YSZ tube so that the crucible could slip over the end of the tube. This improved the quality of the seal, since it was no longer a butt joint, and it raised the seal above the level of the tin. Further, the seal was above the end of the anode inlet tube, so any oxygen leaking into the cell is blown out the exhaust line. The graphite rod (and attached silver current/potential wires) was replaced with two pure rhenium wires (one for current, one for potential) submerged directly into the tin bath. The graphite was replaced because the graphite rod was found to have partially crumbled and oxidized after small intervals of unexpected equipment failure that caused large current spikes to be applied to the sample. Additional enhancements in the cell design include (1) adding a thermocouple (type K, sheathed in an alumina tube) attached to a translation stage for probing the temperature through the tin bath and (2) attaching the anode inlet tube and current/potential wires to a second translation stage to allow for insertion and extraction of the rod during the experiment.

Fig. 7(b) shows a typical current response from the improved cell design under the same conditions used in Fig. 7(a). The smaller current signal for the sample in (b) compared with that in (a) is due to the thicker YSZ layer of the crucible (~1.5 mm) compared to that of the button cell (~150 μm) used in the different cell designs. While the current is smaller, the noise level is significantly reduced. A single potential step cycle is shown, and not an average of 10 cycles as shown in Fig. 7(a). The oxygen diffusion coefficient for tin under hydrogen (with 3% H_2O) at 800 °C and 900 °C was calculated to be 5.4×10^{-5} and 8.9×10^{-5} $cm^2\ s^{-1}$, respectively. This value is higher, although within an order of magnitude, of that shown in the literature by Chou et al. (7.5×10^{-5} and 1.0×10^{-4} $cm^2\ s^{-1}$) [38], Sears et al. (9.2×10^{-5} and 1.2×10^{-4} $cm^2\ s^{-1}$) [39], and Ramanarayanan and Rapp (5.2×10^{-5} and 6.6×10^{-5} $cm^2\ s^{-1}$) [40].

While the oxygen diffusion coefficients calculated in this work do not vary significantly from those previously reported in literature, one might ask if the presence of hydrogen may significantly affect the calculated diffusion coefficient, as previous experiments were performed in an inert atmosphere. Hydrogen is reported to be insoluble in tin, although there is some discrepancy between Refs. [16,19,41,42]. The most common metals reference books cite the work by Bever and Floe [19] that, while questionable, calculated the solubility of hydrogen in tin at 1000 °C to be 0.04 cm^3 of H_2 at 1 atm. per 100 g of Sn. This amount is equivalent to 9×10^{-5} at% H in Sn, more than two orders of magnitude than the oxygen solubility limits calculated in this present work. Bever and Floe contradicted earlier, even less reliable data from Iwase [43] that reported much higher hydrogen solubility limits: 0.014 at% H in Sn at ~1000 °C. This value is still at least an order of magnitude smaller than the solubility limit of oxygen; however, one would also have to consider the mobility of hydrogen atoms. There are no reported values for the diffusion coefficient of hydrogen in liquid tin; however, Sacris and Parlee did measure hydrogen transport in liquid nickel, copper, and silver while attempting to measure it in liquid tin [44]. They estimated that the hydrogen diffusivity in tin would be the fastest of all the tested metals, with silver, the next fastest, having a diffusion coefficient of $\sim 3.89 \times 10^{-2}$ $cm^2\ s^{-1}$ at 800 °C. This value is almost three orders of magnitude larger than the oxygen diffusion coefficient in liquid tin at 800 °C. A larger value should be expected, as hydrogen is smaller and lighter than oxygen. If enough mobile, active hydrogen is present in the tin bath, the effective diffusion path length for oxygen diffusion could be reduced as the oxygen could react with hydrogen before reaching the tin surface. A shorter *effective* diffusion path length would reduce the calculated value of D_o. Potential step measurements with and without hydrogen (i.e., under UHP argon or with carbon-containing fuel) are currently being made to isolate the effect of hydrogen.

A higher diffusion coefficient could also result from convection from within the tin bath. The translatable thermocouple indicated that at 800 °C and 900 °C the tin bath was isothermal, within ±0.5 °C for up to a 1 cm thick layer of tin, so thermal convection should not play a large role. Solutal convection may add to oxygen transport, but it has not been accounted for in these calculations [39]. Mechanical convection may result from the flow of gas blown onto the top of the tin bath. This effect can be isolated by varying the flow rate across the sample (even testing under stagnant gas flow conditions).

To put the oxygen diffusion coefficient D_o values into perspective, one can calculate an oxygen conductivity σ_o at temperature T value using the equation

$$\sigma_o = \frac{c_o z_o^2 e^2 D_o}{kT} \tag{4.1}$$

in which z_o is the charge of the oxygen ion, k is the Boltzmann constant, and c_o is the concentration of the oxygen species within the liquid tin. For example, at 900 °C, using $D_o = 8.9 \times 10^{-5}$ $cm^2\ s^{-1}$ (from experimental data) and $c_o = 0.0018$ mole fraction (from FactSage calculations), then the oxygen conductivity would be 0.034 S cm^{-1}. To compare, the oxygen conductivity of 6 mol% YSZ (the crucible material used in the diffusion coefficient experiments) at 900 °C is 0.08 S cm^{-1}, within the same order of magnitude. For any system in which the tin layer is significantly thicker than the electrolyte layer, the ohmic drop across the tin layer due to oxygen transport will be greater than that due to oxygen transport through the electrolyte. The minimum tin layer thickness is dictated by the wetting characteristics of tin with the electrolyte. As tin does not wet YSZ, a thin tin layer would require a certain amount of pressure or a support layer to force the tin against the YSZ. Likewise, additives can be used to make the tin wet the electrolyte; however, the effect of the additives on the oxygen transport or fuel oxidation kinetics would need to be evaluated. Increasing the rate of oxygen transport through the tin may be accomplished through alloying to increase the oxygen solubility limit and possibly increase the oxygen diffusion coefficient. Careful consideration must be given to selecting alloying elements that will form a liquid, nonvolatile liquid metal and will not form a slag (i.e., will not oxidize) during cell operation.

5. Summary

Liquid metal anode SOFC (LMA-SOFC) technology is being studied by NETL as a means for direct conversion of solid coal to electricity. A detailed assessment for the electrochemical activity and oxygen diffusion within the liquid tin is required for modeling cell performance with respect to cell geometry. Test procedures developed at NETL are being used to characterize the transport behavior of the oxygen in the tin. Analysis of the electrochemical data resulted in oxygen diffusion coefficients through tin at 800 °C and 900 °C that were within the same order of magnitude of previously reported literature values. The oxygen conductivity through the tin, calculated from measured diffusion coefficients and theoretical thermodynamic oxygen solubility limits, is found to be on the same order of that of YSZ. As such, the ohmic loss

due to oxygen transport through the tin layer is significant since the tin layer will probably be much thicker than that of the electrolyte. Oxygen transport through the liquid metal can be enhanced through alloying to increase the oxygen solubility limit; however, the impact on the wetting characteristics of the liquid metal and on the fuel oxidation kinetics needs to be similarly considered. The balance of these properties dictates the ultimate design of a practical LTA-SOFC system.

Acknowledgements

The authors wish to thank Rich Pineault for assisting with the design and installation of experimental hardware and Dr. Nguyen Minh for helpful comments made to support this work.

References

[1] International Energy Agency, World Energy Outlook 2008, OECD/IEA, 2008.
[2] United States Department of Energy, Energy Information Administration, Electric Power Monthly November 2009, 2009.
[3] J. Gale, S. Bachu, O. Bolland, Z. Xue, Int. J. Greenhouse Gas Control 1 (2007).
[4] United States Department of Energy, Office of Fossil Energy, National Energy Technology Laboratory, Carbon Sequestration Technology Roadmap and Program Plan, 2007.
[5] T. Tao, in: S.C. Singhal, J. Mizusaki (Eds.), SOFC-IX, Quebec City, Canada, The Electrochemical Society, Inc, Pennington, NJ, USA, 2005, pp. 353–362.
[6] F.N. Cayan, M.J. Zhi, S.R. Pakalapati, I. Celik, N.Q. Wu, R. Gemmen, J. Power Sources 185 (2008) 595–602.
[7] J. Bao, G.N. Krishnan, P. Jayaweera, K.H. Lau, A. Sanjurjo, J. Power Sources 193 (2009) 617–624.
[8] Z. Cheng, S.W. Zha, M.L. Liu, J. Power Sources 172 (2007) 688–693.
[9] T. Tao, W.A. McPhee, M.T. Koslowske, L.S. Bateman, M.J. Slaney, J. Bentley, ECS Trans. 12 (2007) 681–690.
[10] T. Tao, M. Slaney, L. Bateman, J. Bentley, ECS Trans. 7 (2007).
[11] W.A.G. McPhee, M. Boucher, J. Stuart, R.S. Parnas, M. Koslowske, T. Tao, B.A. Wilhite, Energy Fuels 23 (2009) 5036–5041.
[12] M.T. Koslowske, W.A. McPhee, L. Bateman, M. Slaney, J. Bentley, T. Tao, Adv. Solid Oxide Fuel Cells V 30 (2009).
[13] T. Tao, W. McPhee, M. Koslowske, J. Bentley, M. Slaney, L. Bateman, ECS Trans. 25 (2009) 1115–1124.
[14] P.A. Cox, The Elements: Their Origin, Abundance, and Distribution, Oxford University Press, USA, 1989.
[15] US Geological Survey Minerals Information Team, Mineral Commodity Summaries 2010, U.S. Government Printing Office, Reston, VA, 2010.
[16] P.J. Smith, Chemistry of Tin, second ed., Blackie Academic & Professional, 1998.
[17] L.W. Wang, Q.S. Mei, J. Mater. Sci. Technol. 22 (2006) 569–571.
[18] N. Cusack, J.E. Enderby, Proc. Phys. Soc. Lond. 75 (1960) 395–401.
[19] M.B. Bever, J. Member, C.F. Floe, Trans. Am. Inst. Min. Metall. Eng. 156 (1944) 149–159.
[20] E. Ricci, L. Nanni, A. Passerone, Philos. Trans. R. Soc. Lond. Ser. a—Math. Phys. Eng. Sci. 356 (1998) 857–869.
[21] M. Hansen, K. Anderko, Constitution of Binary Alloys, second ed., McGraw-Hill, New York, 1958.
[22] S. Cahen, N. David, J.M. Fiorani, A. Maitre, M. Vilasi, Thermochim. Acta 403 (2003) 275–285.
[23] T.N. Belford, C.B. Alcock, Trans. Faraday Soc. 61 (1965) 443.
[24] C.W. Bale, P. Chartrand, S.A. Degterov, G. Eriksson, K. Hack, R. Ben Mahfoud, J. Melançon, A.D. Pelton, S. Petersen, Calphad 26 (2002) 189–228.
[25] C.W. Bale, E. Bélisle, P. Chartrand, S.A. Decterov, G. Eriksson, K. Hack, I.H. Jung, Y.B. Kang, J. Melançon, A.D. Pelton, C. Robelin, S. Petersen, Calphad 33 (2009) 295–311.
[26] E.H.P. Cordfunke, Thermochemical Data for Reactor Materials and Fission Products, North-Holland, Amsterdam, 1990.
[27] I. Barin, O. Knacke, O. Kubaschewski, Thermochemical Properties of Inorganic Substances, Springer-Verlag, New York, 1977.
[28] T.J. Heames, D.A. Williams, N.E. Bixier, A.J. Grimley, C.J. Wheatley, N.A. Johns, P. Domagala, L.W. Dickson, C.A. Alexander, L. Osborne-Lee, S. Zawadzki, J. Rest, A. Mason, R,Y. Lee, Victoria: A Mechanistic Model of Radionuclide Behaviour in the Reactor Coolant System Under Severe Accident Conditions, Sandia National Laboratories (NUREG/CR-5545, SADN90-0756, Rev.1), (Dec. 1992).
[29] D.D. Wagman, W.H. Evans, V.B. Parker, I. Halow, S.M. Bailey, R.H. Schumm, Selected Values of Chemical Thermo-Dynamic Properties, in, United States Department of Commerce Editor. (1968–1981).
[30] I. Barin, Thermochemical Data of Pure Substances, VCH, Weinheim, Germany, 1989.
[31] I.M.B. Nielsen, C.L. Janssen, M.D. Allendorf, J. Phys. Chem. A 107 (2003) 5122–5127.
[32] M.G. Bonicelli, G. Ceccaroni, F. Gauzzi, G. Mariano, Thermochim. Acta 430 (2005) 95–99.
[33] Z.M. Jarzebski, J.P. Marton, J. Electrochem. Soc. 123 (1976) C299–C309.
[34] J.H. Lee, S.J. Park, K. Hirota, J. Am. Ceram. Soc. 73 (1990) 2771–2774.
[35] B. Kamp, R. Merkle, R. Lauck, J. Maier, J. Solid State Chem. 178 (2005) 3027–3039.
[36] P.S. Peercy, B. Morosin, Phys. Rev. B 7 (1973) 2779–2786.
[37] H.S. Carslaw, J.C. Jaeger, Conduction of Heat in Solids, second ed., Oxford University Press, Oxford, 1959.
[38] H. Chou, T.C. Chow, S.F. Tsay, H.S. Chen, J. Electrochem. Soc. 142 (1995) 1814–1819.
[39] B. Sears, T.J. Anderson, R. Narayanan, A.L. Fripp, Metall. Trans. B—Process Metall. 24 (1993) 91–100.
[40] T.A. Ramanarayanan, R.A. Rapp, Metall. Trans. 3 (1972) 3239–3246.
[41] C.J. Smithells, Smithells Metals Reference Book, eighth ed., Elsevier Butterworth-Heinemann, Boston, 2001.
[42] B.T.K. Barry, C.J. Thwaites, Tin and its Alloys and Compounds, Halsted Press, New York, 1983.
[43] K. Iwase, Science Reports of the Tohoku Imperial University, vol. 15, 1926.
[44] E.M. Sacris, N.A.D. Parlee, Metall. Trans. 1 (1970) 3377.
[45] R.C. Sharma, Y.A. Chang, J. Phase Equilibr. 7 (1986) 269–273.